inter.noise 2000
The 29th International Congress and Exhibition on Noise Control Engineering
27-30 August 2000, Nice, FRANCE

I-INCE Classification: 7.6

FINITE DIFFERENCE SOLUTION OF SOUND PROPAGATION OVER POROUS GROUND

H. Dong*, J.M. Hovem*, L.R. Hole, C. Madshus*****

* Department of Telecommunications/Acoustics, Norwegian University of Science and Technology, Dept. of Telecommunications/Acoustics, NTNU, N-7491, Trondheim, Norway

** Norwegian Defence Construction Servise, Oslo mil/Akershus, N-0015, Oslo, Norway

*** Norwegian Geotechnical Institute, Sognsveien 72 P.O.Box 3930 Ullevaal Station, N-0806, Oslo, Norway

Tel.: 4773590465 / Fax: 4773591412 / Email: dong@tele.ntnu.no

Keywords:
FINITE DIFFERENCE, SOUND, PROPAGATION

ABSTRACT

This paper presents an axis-symmetric pressure-velocity finite-difference formulation (PV-FD) for sound propagation over ground based on Biot theory. Some typical results of simulation are presented and comparisons with the measurements during airblast tests performed in Haslemoen, Norway are presented in order to verify the proposed model. The model can also handle range-dependent and topographic ground. Representative results are presented for two cases of uniform ground with local alterations: one where a region of the ground is assigned a higher permeability, and the other where the same zone is replaced by stiffer zone. The case with a hill above homogeneous poro-elastic ground is also considered. The developed numerical code is shown to be a practical tool for simulating complicated ground features and a useful tool in calibrating empirical sound prediction models.

1 - INTRODUCTION

In recent years investigators have used different approaches to study the propagation of impulse noise. The applied methods have included complex impedance ground representation (Don and Cramond, 1987), rigid-porous approximation (Attenborough, 1992), frequency-wave number integration technique (Schmidt, 1997) and viscoelastic approach (Hole, 1998). Hole *et al.* (1998) have used frequency-wave number integration method for the simulation of low-frequency noise and ground vibration in the Norwegian airblast tests in Haslemoen.

This paper presents an axis-symmetry finite difference formulation for modelling sound propagation in seismo-acoustic media. The numerical simulations comprising synthetic time histories are shown and comparisons are presented with the measurements during airblast tests performed in Haslemoen, Norway and the simulations by the frequency-wave number FFP model OASES (Hole *et al.*, 1998). The influence of range-dependent parameters on sound propagation is considered for highlighting the effect of the various non-homogeneities. The snap-shots of air pressure and ground particle velocities are presented to highlight the overall features of sound propagation over a non-homogeneous poro-elastic medium. In particular, the generation of Mach surfaces in the ground due to the super-seismic propagation of sound wave is demonstrated.

2 - THEORY AND NUMERICAL METHOD

An axis-symmetry cylindrical coordinate system is considered and a point source is located on z-axis above the ground. The equation for air pressure P is

$$\partial_{tt} P(\mathbf{x},t) / \left(\rho_0 V_0^2\right) + \nabla \cdot \left(\nabla P(\mathbf{x},t) / \rho_0\right) = g(t)\,\delta(\mathbf{x}-\mathbf{x}_0) \tag{1}$$

where $\delta(\mathbf{x})$ is the Kronecker Delta, $g(t)$ defines the time variation of the point source, $\mathbf{x}_0$ specifies the position of the point source, and V_0 and ρ_0 are the sound speed and mass density of the atmosphere. In poro-elastic ground the velocity of the frame $\mathbf{u}$ and the relative velocity of the pore fluid $\mathbf{w}$ satisfy Biot theory (1956)

$$\begin{array}{c} \rho_f \ddot{\mathbf{u}} + e\rho_f/\phi \ddot{\mathbf{w}} + \eta/\kappa \dot{\mathbf{w}} = \mathbf{D}_1(\mathbf{u}; \alpha M) + \mathbf{D}_1(\mathbf{w}; M) \\ \rho \ddot{\mathbf{u}} + \rho_f \ddot{\mathbf{w}} = \mathbf{D}_1(\mathbf{u}; H - 2\mu) + \mathbf{D}_2(\mathbf{u}; \mu) + \mathbf{D}_1(\mathbf{w}; \alpha M) \end{array} \tag{2}$$

where for simplicity two vector differential operators $\mathbf{D}_1$ and $\mathbf{D}_2$ are used and defined by

$$\begin{array}{c} \mathbf{D}_1(\mathbf{f}; A) = A \nabla\nabla \cdot \mathbf{f} + \nabla B \nabla \cdot \mathbf{f} \\ \mathbf{D}_2(\mathbf{f}; B) = B \nabla\nabla \cdot \mathbf{f} + B\nabla^2 \mathbf{f} + \nabla B \times (\nabla \times \mathbf{f}) + 2(\nabla B \cdot \nabla)\mathbf{f} \end{array} \tag{3}$$

In equation (2), ϕ and e are the porosity and tortuosity of the porous medium, respectively. The poro-elastic mass parameters are identified by $\rho = \phi\rho_f + (1-\phi)\rho_s$ where ρ_s and ρ_f are the mass densities of the solid grains and the pore fluid, respectively. κ is the permeability and η is the viscosity of the pore fluid, μ is the shear modulus of the solid frame. $\alpha = 1 - K_b/K_s$ and $M = (\phi/K_f + (\alpha - \phi)/K_s)^{-1}$, where K_b, K_s and K_f are the bulk moduli of the solid frame, solid grains and pore fluid, respectively, and $H = K_b + 4\mu/3 + \alpha^2 M$. Furthermore, $\mathbf{w} = \phi(\mathbf{U} - \mathbf{u})$ where $\mathbf{U}$ is the velocity of pore fluid. On the interfaces between air and porous medium, pressure and velocities should satisfy the boundary conditions

$$\left\{ \begin{array}{l} -\dfrac{1}{\rho_f}\partial_j P_f = \partial_t (u_j + w_j) \\ -\partial_t P_f = \alpha M \nabla \cdot \mathbf{u} + M \nabla \cdot \mathbf{w} \\ -\partial_t P_f = (H - 2\mu)\nabla \cdot \mathbf{u} + \alpha M \nabla \cdot \mathbf{w} + 2\mu \partial_j u_j \\ 0 = \mu(\partial_r u_z + \partial_z u_r) \end{array} \right. \Rightarrow \left\{ \begin{array}{ll} j = z & , z = \text{constant} \\ j = r & , r = \text{constant} \end{array} \right. \tag{4}$$

Defining the finite-difference operator

$$\Omega_j(\mathbf{f}; A) = \mathbf{F}_d \cdot \{\mathbf{D}_j(\mathbf{f}; A)\}, \ j = 1, 2 \tag{5}$$

where $\mathbf{F}_d \cdot \{\}$ indicates a finite difference representation of the variable inside the brackets. Using this operator equation (2) can be expressed as

$$\begin{array}{c} \mathbf{F}_d \cdot \{\rho_f \ddot{\mathbf{u}} + e\rho_f/\phi \ddot{\mathbf{w}} + \eta/\kappa \dot{\mathbf{w}}\} = \Omega_1(\mathbf{u}; \alpha M) + \Omega_1(\mathbf{w}; M) = \Psi_1^k \\ \mathbf{F}_d \cdot \{\rho \ddot{\mathbf{u}} + \rho_f \ddot{\mathbf{w}}\} = \Omega_1(\mathbf{u}; H - 2\mu) + \Omega_2(\mathbf{u}; \mu) + \Omega_1(\mathbf{w}; \alpha M) = \Psi_2^k \end{array} \tag{6}$$

where Ψ_1^k and Ψ_2^k contain only spatial derivatives that need to be evaluated at the current time $t = k\Delta t$ in a time marching algorithm. k is time index and Δt is the increment of time. Using the central finite difference in time on the left-hand side of equation (6) and rearranging the terms, we get

$$\begin{array}{c} a_{11}\mathbf{u}^{k+1} + a_{12}\mathbf{w}^{k+1} = \mathbf{b}_1 + (\Delta t)^2 \Psi_1^k \\ a_{21}\mathbf{u}^{k+1} + a_{22}\mathbf{w}^{k+1} = \mathbf{b}_2 + (\Delta t)^2 \Psi_2^k \end{array} \tag{7}$$

where a_{ij} is the coefficient of $\mathbf{u}^{k+1}$ and $\mathbf{w}^{k+1}$, and $\mathbf{b}_j$ includes the values of $\mathbf{u}$ and $\mathbf{w}$ in the time $k\Delta t$ and $(k-1)\Delta t$. Interface equations have been treated using an integration technique by Dong et al. (1999). The absorbing boundary conditions and the stability of the finite-difference schemes have been studied by several authors (Reynolds, 1978 and Marfurt, 1984).

3 - NUMERICAL RESULTS

We are discussing three groups of ground parameters and they are given in Table 1. Group I corresponds to a layered ground. Case A is a homogeneous poro-elastic ground (Group II). Case B and Case C are similar to Case A except for the inclusion of a higher permeability ($\kappa = 10^{-8}$ m^2) region and a stiffer (by 50%) region between 100 to 150m, respectively. Case D defers from Case A by the addition of an elastic rectangular hill (Group III) of height 8.65m on the ground in the range 100 to 150. In addition, it is assumed that f=0.44, dynamic viscosity of pore air η=1.74 $\times 10^{-5}$, tortuosity e=1.25, sound speed V_0=340m/s, mass density of air ρ_0=1.2 kg/m^3 in all of the cases. The source function is similar to that of Hole *et al.* (1998), and the centre frequency is 30 *Hz*.

Group		H (m)	ρ_f (kg/m^3)	K_f (10^6 Pa)	ρ_s (kg/m^3)	K_s (10^6 Pa)	K_b (10^6 Pa)	μ_b (10^6 Pa)	κ (10^{-10} m^2)
I	1	0.5	1.2	0.13	2700	9060	60.7	25.5	100
	2	0.5	-	-	1500	68.4	68.4	25.35	-
	3	1.5	-	-	1500	72.0	72.0	29.4	-
	4	2.5	-	-	1500	83.85	83.85	33.75	-
	5	5.0	-	-	1600	96.6	96.6	38.4	-
	6	10.0	-	-	1700	180.0*	180.0*	60.0*	-
	7	∞	**-**	**-**	1800	281.25*	281.25*	93.75*	-
II		∞	1.2	0.13	2700	9060	60.7	25.5	1.0
III		∞	-	-	1500	62.4	62.4	29.4	-

Table 1: Parameters of models used in simulations (* for numerical considerations these parameters are set lower than those used by Hole et al, 1998).

Fig. 1 displays comparisons of different time histories of overpressure in the air and vertical particle velocity in the ground using parameter Group I in Table 1. The results are from the finite-difference model, frequency-wave number model OASES (Hole *et al.*, 1998) and the measurements from the Norwegian blast tests. The sensors are at distances of 195m and 260m from the blast site and are positioned 2m above ground for overpressure and on the ground surface for vertical particle velocity. Examination of the plots for the various overpressure data shows a fairly good accord in the amplitudes and arrival times between the cases. Moreover, the simulations reveal a decrease in the dominant frequency of the sound with distance as observed in the experimental data. For the ground response, the arrivals and amplitudes of the first peaks are almost the same in the two calculation models. However, the amplitudes of the subsequent peaks (resulting from reflected and refracted waves in the ground) are different. The difference could be partly due to absence of body wave attenuation.

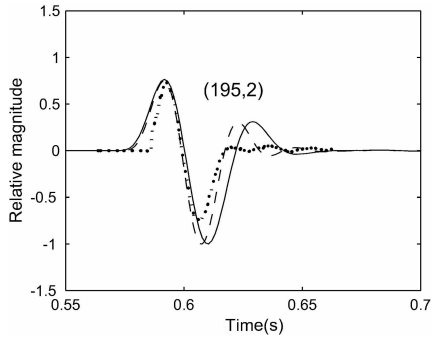

(a): Upper panel for pressure at 195m.

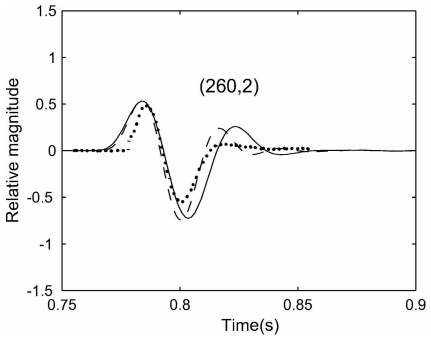

(b): Upper panel for pressure at 260m.

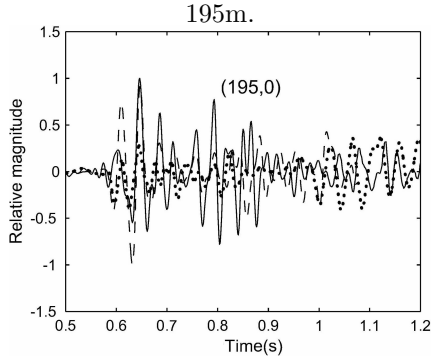

(c): Lower panel for ground velocity at 195m.

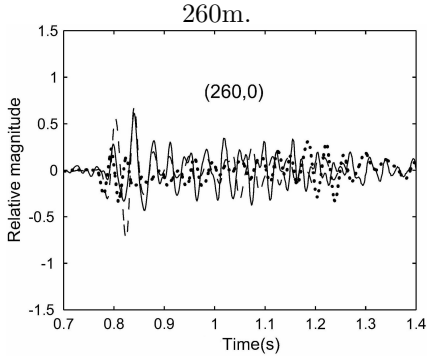

(d): Lower panel for ground velocity at 260m.

Figure 1: Comparison between finite-difference model (solid line), OASES (dashed line) and experimental data (dotted line).

To discern the influence of permeability of the porous layer on the sound absorption and the induced ground vibration, different simulations were carried out by decreasing the permeability by 100 times,

that is to $\kappa = 10^{-10}$ m^2. Fig. 2 shows a comparison between the results of the overpressure at 2m above ground (Fig. 2a) and vertical vibration on ground surface (Fig. 2b) with different permeability. These results support the conclusions by Hole *et al.* (1998) in that the amplitude of air pressure and the peak particle velocity decrease with permeability. Furthermore, the dominant frequencies in both overpressure and ground vibration decrease as permeability increases.

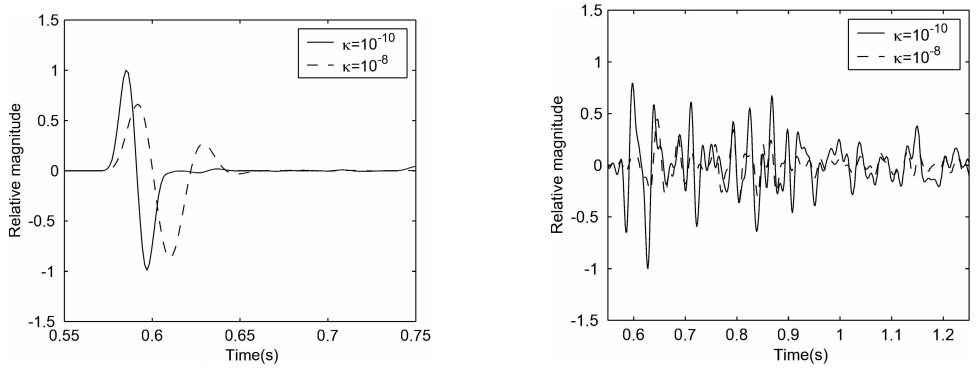

(a): Pressure at 2m above ground. **(b):** Vertical velocity on ground surface.

Figure 2: Comparison between the results with different permeability at 195m from the source (solid line for $\kappa = 10^{-10}$ m^2 and dashed line for $\kappa = 10^{-8}$ m^2.

Fig. 3 displays the time histories of overpressure at 2m above ground and vertical velocity on the ground surface, at distances of 80 and 160m from the source. The results are plotted for three cases: Case A (dashed line), Case B (dotted line) and Case C (solid line). As expected for Fig. 3a, the first arrivals at 80m are identical in the three cases. At 160m, however, both the amplitude and the dominant frequency for Case B reduce. This is due to the passage of the sound over the more permeable zone in Case B. In Fig. 3b at 160m, the amplitude of the first peak in Case C is different from the other two cases due to the coincidence of the direct wave and P-wave. In addition, there is a second reflected P-wave from the stiff zone at about 0.7s.

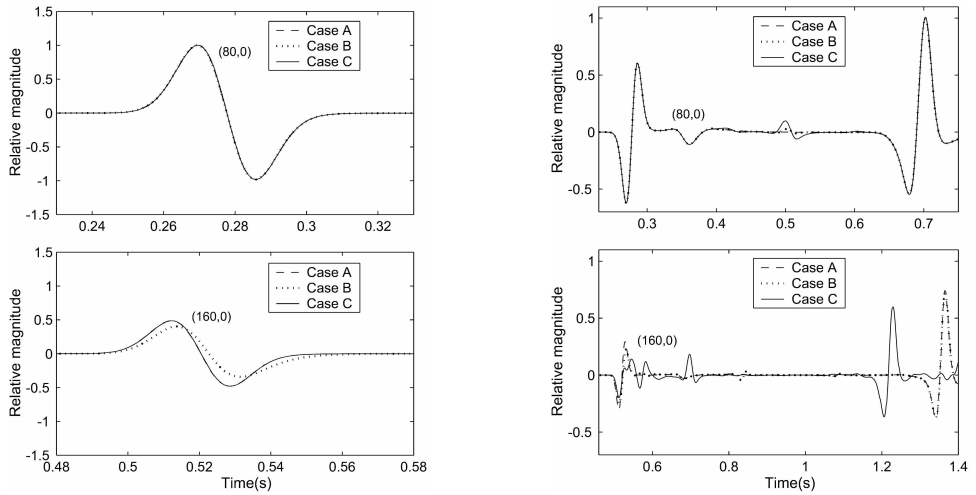

(a): At 2m above ground. **(b):** On ground surface.

Figure 3: Comparison of overpressures and vertical velocities among case A (dashed line), case B (dotted line) and case C (solid line) at distances of 80m (upper panels) and 160m (lower panels).

A global picture of sound propagation and its interaction with the ground can be obtained by snap-shots. Fig. 4 presents the snap-shots of overpressure and vertical ground velocity normalised by overpressure at a fixed time: (a) the layered model (Group I) and (b) a homogeneous poro-elastic ground with a hill (Case D). The former shows a complicated deformation pattern in the ground resulting from the reflection and refraction of P- and S-waves as well as surface waves. A careful examination for this case shows the presence of Mach surfaces in the ground (although not quite straight due to ground layering).

Because the velocities of P- and S-waves in the upper layers of the ground are lower than the sound speed, a super-seismic condition, characterized by the generation of two Mach surfaces, is realized. Fig. 4b shows, on the other hand, large wave reflections from the hill. In particular, there are two pairs of Mach surfaces, one due to the incident body waves and the other related to the reflected waves from the hill. This visual feature is one of the most powerful attributes of the finite difference model that allows one to gain insight into the mechanism of generation and propagation of waves.

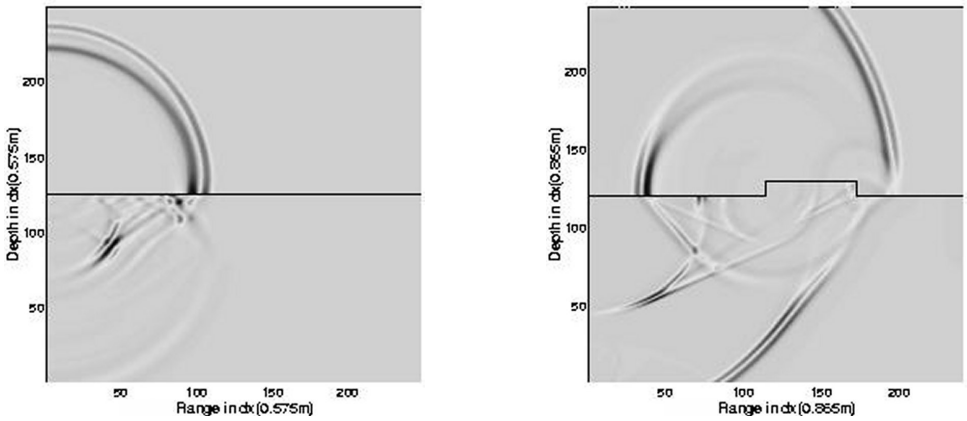

(a): Layered ground at 0.1929 s. **(b):** Ground with a hill at 0.543 s.

Figure 4: Snapshots of overpressure and vertical ground velocity normalized by overpressure.

4 - CONCLUSIONS

A pressure-velocity finite-difference technique is used to simulate sound propagation over a ground with different properties. Numerical simulations are carried out for both overpressure in air and particle velocity in the ground. Comparisons are presented with the experimental data and the results by a frequency-wave number integration method. The results from different ground models are compared and the influence of range-dependent and topographic properties on sound propagation is presented. Typical snap-shots of overpressure and ground velocity are presented to illustrate the overall features of sound propagation over porous media.

REFERENCES

1. **F. G. Don and A. J. Cramond**, Impulse propagation in a neutral atmosphere
2. **K. Attenborough**, Ground parameter information for propagation modeling
3. **H. Schmidt**, *OASES version 2.0, application and upgrade notes*
4. **L. R. Hole**, An experimental and theoretical study of propagation of acoustic pulses in a strongly refracting atmosphere
5. **L. R. Hole, A. M. Kaynia and C. Madshus**, Measurement and simulation of low frequency impulse noise and ground vibration from airblasts
6. **M. A. Biot**, Theory of elastic waves in a fluid-saturated porous rock: I. Low-frequency range
7. **H. Dong, K. Wang and J. M. Hovem**, A stable integration technique for the interface conditions between two different media in the finite-difference method
8. **A. C. Reynolds**, Boundary conditions for the numerical solution of wave propagation problems
9. **K. J. Marfurt**, Accuracy of finite-difference and finite-element modeling of the scalar and elastic wave equations